Automatic Kidney Segmentation in CT Images based on Multi-atlas Image Registration

Guanyu YANG, *IEEE Member,* Jinjin GU, Yang CHEN, *IEEE Member,* Wangyan LIU, Lijun TANG, Huazhong SHU, *IEEE Member*, Christine TOUMOULIN

***Abstract*—Kidney segmentation is an important step for computer-aided diagnosis or treatment in urology. In this paper, we present an automatic method based on multi-atlas image registration for kidney segmentation. The method mainly relies on a two-step framework to obtain coarse-to-fine segmentation results. In the first step, down-sampled patient image is registered with a set of low-resolution atlas images. A coarse kidney segmentation result is generated to locate the left and right kidneys. In the second step, the left and right kidneys are cropped from original images and aligned with another set of high-resolution atlas images to obtain the final results respectively. Segmentation results from 14 CT angiographic (CTA) images show that our proposed method can segment the kidneys with a high accuracy. The average Dice similarity coefficient and surface-to-surface distance between segmentation results and reference standard are 0.952 and 0.913mm. Furthermore, the kidney segmentation in CT urography (CTU) and CTA images of 12 patients were performed to show the feasibility of our method in CTU images.**

I. Introduction

Kidney segmentation in CT images is an important preprocessing step for computer-aided diagnosis or treatment in urology. Some useful information, such as renal volume, anatomy of kidney, etc., can be obtained after segmenting kidney from CT images. Several approaches have been presented for kidney segmentation in CT images. Spiegel [1] introduced an algorithm based on 3D active shape model (ASM). Khalifa [2] proposed a level-set method which combined a probabilistic shape prior and a novel stochastic speed function. These two methods were applied semi-automatically with a manual initialization. Lin [3] developed an automatic method based on adaptive region growing to extract kindey within a region-of-interest (ROI). But this method mainly depended on the assumption of homogeneity of image intensity. It is not suitable for the image with large variation of image intensity within the region of kidney. Recently, Cuingnet [4] developed a coarse-to-fine approach for kidney segmentation from contrast and non-contrast CT images. A random forest classifier gave coarse kidney segmentation first. Then the implicit template model was applied to refine the segmentation result. However, 54 datasets with manually drawn contours were used to perform classifier training. Manual delineation of kidney in such a large number of 3D images was a time consuming task.

In this paper, we implement an multi-atlas based method to obtain a coarse-to-fine segmentation of kidney in CT images. This method mainly relies on performing image registration between patient image and multiple atlas images. Experimental results demonstrate that our proposed multi-atlas based method can generate accurate segmentation results of kidneys in CT images.

This research was supported by National Natural Science Foundation under grants (81101104), National Basic Research Program of China under grant (2011CB707904) and Natural Science Foundations of Jiangsu Province (BK2012743) and Technology Foundation for Selected Overseas Chinese Scholar, Department of Human Resources and Social Security of Nanjing..

G.Y. Yang, J. Gu, Y. Chen and H.Z. Shu are with Lab of Image Science and Technology, Key Laboratory of Computer Network and Information Integration (Southeast University), Ministry of Education. and Centre de Recherche en Information Biomedicale Sino-Francais (LIA CRIBs) (Corresponding author: G.Y. Yang, phone: 0086-25-83794249; e-mail: yang.list@ seu.edu.cn).

W. Liu and L. Tang are with Dept. of Radiology, the First Affiliated Hospital of Nanjing Medical University, Nanjing, China.

C. Toumoulin is with INSERM-U1099, LTSI, Université de Rennes 1, Rennes, F-35000, France and Centre de Recherche en Information Biomédicale Sino-Français (LIA CRIBs).

II. Methodology

A. Kidney segmentation using multi-atlas image registration

In the multi-atlas based segmentation method, the patient dataset is aligned with each atlas image to map the reference labels of the atlas images to the patient image. Then, the deformed reference labels from each atlas image can be fused together to generate final segmentation result by a specified fusion criterion.

This segmentation method mainly relies on the image registration which is defined as an optimization problem to find an optimal transformation $\hat{T}$ between a fixed patient image $I_P(x)$ and a moving atlas image $I_A(x)$,

$$\hat{T} = \arg\min_{T} C(I_P(x), I_A(T(x))) \quad (1)$$

in which $T(x)$ is transformation function which deforms $I_A(x)$ to spatially align with $I_P(x)$. In this paper, affine and B-spline non-rigid transformations are employed to ensure accurate matching. C is the cost function to measure the dissimilarity between $I_P(x)$ and deformed $I_A(T(x))$. C is minimized iteratively by an optimization algorithm. Mutual information (MI) defined in [5] is used to measure the dissimilarity in this paper. The cost function is optimized by adaptive stochastic gradient descent method [6]. Considering the computational

cost in the image registration with multiple atlas images, some techniques are applied to improve the computation time. First, a randomly sampled subset of image voxels is selected to measure the dissimilarity cost C in each iteration. The number of voxels in the subset is set to 2048 in this paper. Secondly, a multi-resolution strategy based on Gaussian pyramid is used during the registration process.

However, if we only used the whole patient image to match with the atlas images as applied in the most of atlas-based methods [7, 8], the kidneys could not be segmented accurately. The main reason is that the kidneys are not large dominant organs in the abdominal CT images. Strong boundaries of body, spine and rib cage, etc. influence the dissimilarity measure during the registration when we perform registration on the whole image. In this case, the labels of kidneys in the atlas images cannot be mapped onto the region of kidney in the patient image accurately. Therefore, in this paper, we develop a two-step method to generate a coarse-to-fine kidney segmentation. The framework of our proposed method is displayed in Fig.1. In the first step, the patient CT image is down-sampled and matched with the low-resolution atlas images $A_i^L (i = 1, ..., N)$ to obtain the coarse segmentation of left and right kidney simultaneously. Two region-of-interests (ROIs) are defined automatically by the bounding boxes of the segmented regions to locate the left and right kidneys in the patient image. In the second step, kidneys are cropped from the original patient image by two ROIs acquired in the previous step. Then the cropped patient images are registered with the high-resolution atlas images $A_j^H (j = 1, ..., M)$. Because the kidney is the major structure in the cropped images, the kidneys in the atlas image and the patient image can be matched more accurately in this step. Therefore, a fine segmentation result is obtained finally.

Different registration strategies are applied in these two steps. In the first step, affine transformation is estimated firstly to align the patient image and atlas image approximately. B-spline non-rigid transformation follows to refine the spatial transformation. In the second step, only B-spline non-rigid registration is performed due to the relative small deformations between the cropped patient image and the atlas image.

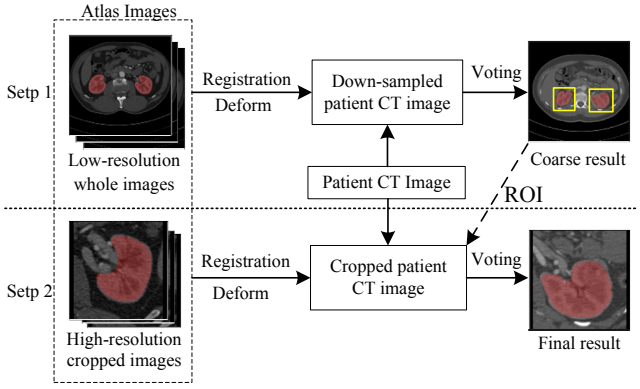

Fig. 1. Framework of our proposed method.

In both steps, the limitation of iteration times in the optimization of cost function C is fixed to 500. A cubic B-spline interpolator is used to estimate the image intensities at non-voxel positions. The B-spline grid is defined by control points with 16 mm interval. The deformed labels obtained from all atlas images are merged together by majority voting (MV) to generate the segmentation result.

B. Building multiple atlas images

Eight abdominal CT angiographic (CTA) images acquired by Siemens dual-source 64-slice CT were selected to generate atlas images. Contrast media was injected during the image acquisition to highlight the renal arteries, cortex and tumor regions. The size of axial image is 512×512. The average pixel size is 0.63 mm^2 and the distance between two axial slices is 0.5mm. The images were interpolated linearly to generate isotropic volumetric images. Two-dimensional contours of left and right kidneys in every 15 axial slices were obtained by an semi-automatic method based on Snake[9]. All the 2D contours then were checked by a radiologist and corrected manually if needed. Finally, the three-dimensional reference label image of the kidneys were defined by interpolating implicit surfaces according to these 2D contours [10]. In Fig.2, the manually corrected 2D contours and 3D label image of the kidneys in one atlas image are displayed in 3D.

Fig. 2 Manually corrected 2D contours of kidney (in red) and 3D labels of kidney (overlapped in yellow).

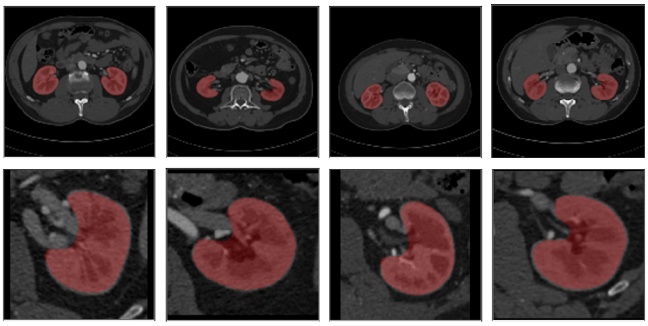

Fig. 3 Axial slices of four atlas images are displayed. Low-resolution whole images and high-resolution cropped images are displayed in the first and the second row respectively. The labels of kidney in the images are overlapped in red.

As mentioned in Section 2.1, the proposed method in this paper relies on the atlas images which are composed by two

subsets, low-resolution whole images (A^L) and high-resolution cropped images (A^H). In this paper, N and M are equal to 8 respectively. The low-resolution whole images in A^L are generated by down-sampling the original images and label images with a factor of 4. The axial image size is 128×128 after down-sampling. In the second subset A^H, the left and right kidneys are cropped from the original images by the ROIs defined by the labels of the kidneys. The kidneys with large renal tumors or renal cysts are excluded from the subset A^H. Finally, 5 left kidneys and 3 right kidneys are included in A^H. Considering the orientation of left and right kidneys is symmetric about the sagittal plane, the cropped images of right kidney are flipped horizontally to make the kidneys in A^H have the same orientation. In Fig. 3, four of eight atlas images including the low-resolution whole images and the high-resolution cropped images are demonstrated.

III. Experimental Results

This kidney segmentation framework based on multi-atlas image registration is implemented in Mevislab (http://www.mevislab.de/). The image registration is performed by an open-source package named ELASTIX [11].

We applied the quantitative evaluation of our proposed method in 14 abdominal CTA images. These images were acquired by Siemens dual-source 64-slice CT with the same imaging protocol as used for atlas images. The pixel size of these CTA images is between 0.59mm^2 to 0.74mm^2. These images were interpolated linearly to generate isotropic volume datasets. The reference standard segmentation of kidneys in these images were generated first by the method described in Section 2.2. After that, our proposed method was applied to extract the regions of kidney automatically. Fig. 4 demonstrates an example of kidney segmentation by our method in axial slices by comparing with the 2D reference contours. In Fig. 4, one can see the segmentation result has a high consistency with the reference contours. In order to evaluate the accuracy of segmentation results quantitatively, Dice similarity coefficient DSC

$$DSC = \frac{2(M \cap R)}{M + R} \tag{2}$$

and mean surface-to-surface distance d_s between the segmentation result M and the reference standard R were computed. Six segmentation results of kidneys with large renal tumors were excluded from this evaluation step because the tumor changed the shape of kidney significantly. It leaded to erroneous image segmentation results as shown in Fig.5 due to the inaccurate image registration. Finally, in total, the segmentation results of 22 kidneys were used to measure the accuracy of our method. The average and the standard deviation of DSC of 22 kidney segmentation results are 0.952 and 0.018 respectively. The mean and standard deviation of d_s are 0.913 mm and 1.06 mm respectively. These values demonstrate that our proposed method has a high accuracy for kidney segmentation.

One thing worth to be mentioned is that the 2D reference contours near renal hilum were delineated with a relatively large bias due to the lack of significant boundary in this region. Thus, as show in Fig. 6, this is one of the main factors that reduces the value of DSC and enlarges the value of d_s.

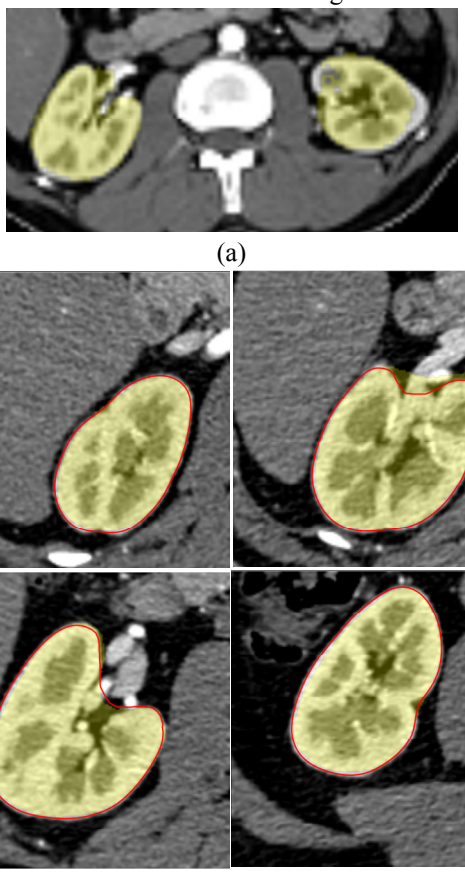

(a)

(b)

Fig. 4. Segmentation results of a kidney by our proposed method. (a) coarse segmentation result obtained in low-resolution image. (b) final result obtained in cropped high-resolution image. The segmented region of kidney is overlapped in yellow. The 2D reference contours are displayed in red.

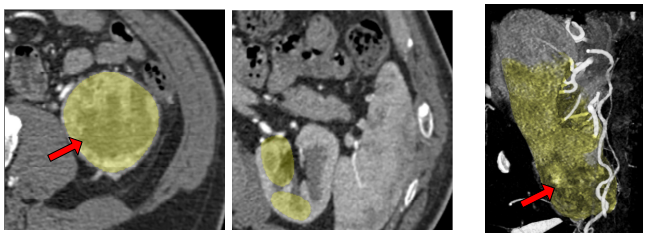

Fig. 5. Segmentation results of a kidney with a large tumor (red arrow) which changed the morphology of kidney significantly. The segmented region of kidney is overlapped in yellow. A part of region of kidney was not extracted correctly.

Considering the dissimilarity measurement based on MI had been applied to many applications of image registration between multi-modality images [12], we tested our

segmentation framework with CT urography (CTU) images. The CTU and CTA images from 12 patients suffered from kidney stones were used as experimental datasets. Different image intensity distribution can be observed in CTA and CTU images. In CTU images, ureters and renal pelvis are highlighted, while in CTA images, arteries and renal cortex are enhanced by contrast media. The kidneys within these datasets were extracted by our proposed segmentation method with the same atlas images as described in Section 2.2 . In Fig. 7, kidney segmentation results both in CTU and CTA images of three patients are displayed. From these results, one can see that the regions of kidney in CTU and CTA are extracted accurately although there are large image intensity difference in the regions of cortex, arteries and ureters of kidney. The segmentation results in CTA and CTU images were reviewed by a radiologist to evaluate their accuracy. Only one right kidney in the CTU image was not segmented correctly because of the boundary between the liver and the kidney was difficult to be distinguished, as displayed in the image of the forth column in Fig.7.

The computation time for one dataset is approximate 5 minutes on a desktop computer with CPU i7-2600 and 8G RAM with multi-threading technique.

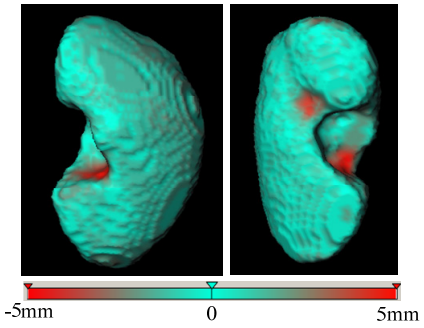

Fig. 6 Distance d_s mapped on the 3D surface of segmentation result. Large d_s can be found in the region of kidney hilum.

IV. Conclusion

In this paper, an automatic method based on multi-atlas image registration for kidney segmentation is presented. The method mainly relies on a two-step multi-atlas image registration to obtain coarse-to-fine segmentation results. In the first step, down-sampled patient image is matched with a set of low-resolution atlas images. A coarse segmentation result is obtained to locate the left and right kidneys in the patient image simultaneously. In the second step, the kidney is cropped from original images and aligned with another set of high-resolution atlas images separately to calculate the fine results. Experimental results in 14 CTA images show that our proposed method can segment the kidney with a high accuracy. The average Dice similarity coefficient and error distance between segmentation results and ground truth are 0.952 and 0.913mm. Additional experiments demonstrate that our segmentation framework is feasible both in CTA and CTU datasets. The segmentation results could be used in the image fusion task between CTA and CTU for invasive operation planning, follow-up treatment evaluation etc. in the future.

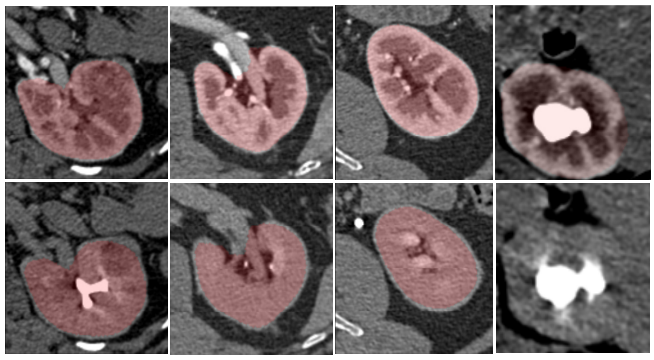

Fig.7 Segmentation results in CTA (the first row) and CTU (the second row) images of four patients are displayed in column respectively. The regions of kidney is overlapped in red. In the forth column, the right kidney in CTU image was not segmented correctly because of the unclear boundary between the liver and the kidney.

References

[1] Spiegel M., Hahn D. A., Daum V., Wasza J., Hornegger, J. "Segmentation of kidneys using a new active shape model generation technique based on non-rigid image registration", Comput. Med. Imag. Grap., vol. 33, no.1, pp.29-39, 2009.

[2] Khalifa F., Elnakib A., Beache G. M., et al. "3D kidney segmentation from CT images using a level set approach guided by a novel stochastic speed function," in Proc.MICCAI 2011. Springer Berlin Heidelberg, pp.587-594, 2011.

[3] Lin D. T., Lei C. C., Hung S. W. "Computer-aided kidney segmentation on abdominal CT images," IEEE Trans. on Inf. Technol. Biomed., , vol. 10, no. 1, pp. 59-65, 2006.

[4] Cuingnet R., Prevost R., Lesage D., et al. "Automatic detection and segmentation of kidneys in 3D CT images using random forests", in Proc. MICCAI 2012. Springer Berlin Heidelberg, pp. 66-74, 2012.

[5] Thévenaz P., Unser M., "Optimization of mutual information for multiresolution image registration," IEEE Trans. Image Process., vol. 9, no.12, pp.2083-2099, 2000.

[6] Klein S., Pluim J.P.W., Staring M., Viergever, M.A., "Adaptive stochastic gradient descent optimization for image registration," Int. J. Comput. Vision, vol. 81, no.3, pp. 227-239, 2009.

[7] Kirişli H.A., Schaap M., Klein S., Neefjes L., Weustink A.C., van Walsum T., Niessen W.J., "Fully automatic cardiac segmentation from 3D CTA data: A multiatlas based approach," Proc. SPIE 7623, 2010.

[8] Asman A. J., DeLisi M. P., Mawn L. A., et al., "Robust non-local multi-atlas segmentation of the optic nerve", SPIE Medical Imaging. International Society for Optics and Photonics, pp. 86691L-86691L-8, 2013.

[9] Kass M., Witkin A., Terzopoulos D., "Snakes: Active contour models", Int. J. Comput. Vision., vol. 1, no. 4, pp. 321-331, 1988.

[10] Turk G., O'brien J.F., "Modelling with Implicit Surfaces that Interpolate," ACM Trans on Graphics, vol.21 no.4, pp.855-873, 2002.

[11] Klein S., Staring M., Murphy K., Viergever M.A., Pluim J.P.W., "Elastix: a toolbox for intensity based medical image registration, " IEEE Trans. Med. Imag., vol.29, no.1, pp.196-205, 2010.

[12] Pluim J.P., Maintz J.A., Viergever M.A., "Mutual-information-based registration of medical images: a survey, ". IEEE Trans. Med. Imag., vol. *22,* no.8, pp.986-1004, 2003.